JACS
JOURNAL OF THE AMERICAN CHEMICAL SOCIETY

COMMUNICATION

pubs.acs.org/JACS

Deviatoric Stress Driven Formation of Large Single-Crystal PbS Nanosheet from Nanoparticles and in Situ Monitoring of Oriented Attachment

Zhongwu Wang,*[,†] Constanze Schliehe,[‡] Tie Wang,[§] Yasutaka Nagaoka,[§] Y. Charles Cao,[§] William A. Bassett,[∥] Huimeng Wu,[⊥] Hongyou Fan,[⊥] and Horst Weller[‡]

[†]Cornell High Energy Synchrotron Source, Wilson Laboratory, and [∥]Department of Earth and Atmospheric Sciences, Cornell University, Ithaca, New York, 14853, United States

[‡]Institute of Physical Chemistry, University of Hamburg, 20146, Hamburg, Germany

[§]Department of Chemistry, University of Florida, Gainesville, Florida 32611, United States

[⊥]Sandia National Laboratories, 1001 University Boulevard SE, Albuquerque, New Mexico 87106, United States

Supporting Information

ABSTRACT: Two-dimensional single-crystal PbS nanosheets were synthesized by deviatoric stress-driven orientation and attachment of nanoparticles (NPs). In situ small- and wide-angle synchrotron X-ray scattering measurements on the same spot of the sample under pressure coupled with transmission electron microscopy enable reconstruction of the nucleation route showing how enhanced deviatoric stress causes ordering NPs into single-crystal nanosheets with a lamellar mesostructure. At the same time that deviatoric stress drives SC(110) orientation in a face-centered-cubic supercrystal (SC), rocksalt (RS) NPs rotate and align their RS(200) and RS(220) planes within the SC(110) plane. When NPs approach each other along the compression axis, enhanced deviatoric stress drives soft ligands passivated at RS(200) and RS(220) surfaces to reorient from a group of SC(110) in-planes to the interspace of SC[110]-normal planes. While the internal NP structure starts a rocksalt-to-orthorhombic transition at 7.1 GPa, NPs become aligned on RS(220) and RS(200) and thus become attached at those faces. The transition-catalyzed surface atoms accelerate the inter-NP coalescing process and the formation of low-energy structure nanosheet. Above 11.6 GPa, the nucleated single-crystal nanosheets stack into a lamellar mesostructure that has a domain size comparable to the starting supercrystal.

Oriented attachment of nanoparticles (NPs) is recognized as a favorable and efficient way to fabricate a variety of linear, chain, zigzag-type one- or two-dimensional nanostructures.[1,2] This newly observed mechanism is different from that of the conventional theory of crystalline nucleation and growth.[3] The classical model describes that tiny crystalline nuclei form in a supersaturated medium and grow larger at the expense of small ones, called *Ostwald* ripening.[4] Unlike the classical mechanism, oriented attachment involves a series of free movements of nucleated NPs that develop a common crystallographic orientation by bridging to nearby NPs. This type of crystal growth starts from an entropy-driven mechanism and then eliminates high surface energy facets and interfaces between NPs, resulting in a coalescence of NPs into a large crystal.[3,4] In addition to extended shape and dimension as well as length scale, nucleated large crystals or transformed building blocks not only display a single-crystal-like structure, but also hold strong size-quantization effects and enhanced properties.[1,2] Given the advantages of these mechanisms for the many promising applications of NPs in biomineralization, sensor and labeling, tough and functional material fabrication, and so forth, it is essential to further understand how NPs interact with media, rotate, and align with each other to ultimately form a single crystal that has either an enlarged size or a soft-molecule/hard-core interconnected mesoscale building block.

Kinetic control of nucleation and growth through oriented attachment includes a series of naturally or experimentally controlled components.[1−4] Natural biomineralization usually offers a neutral hydrothermal environment at ambient pressure and temperature;[5] laboratory conditions can provide additional constraints such as ligand, solvent, light, and temperature. Although environments or media may differ between lab experiments and natural processes, they show analogous oriented attachment mechanisms such as those found in TiO_2 and ZnS.[3] However, extensive investigations on oriented attachments for a wide range of materials depend mostly on direct characterizations of final specimens harvested either in the field or in the lab. This approach, however, is not able to distinguish among the various components that influence the oriented attachment mechanisms. Moreover, a very challenging research objective remains as yet unexplored: development of an in situ monitoring technique to provide direct access to the detailed route by which crystals grow from NPs through oriented attachment mechanisms.

For many NPs with a variety of compositions, surface stress has been recognized as one of the most important features. Surface stress (or surface tension) dramatically increases with decreasing particle size down to 10 nm.[6] According to thermodynamic theory, surface stress acts as a driving force, influencing free movements and interactions of NPs and leading to oriented attachment and ultimate coalescence of NPs. Here, we report the development of a method employing in situ small (SAXS) and wide (WAXS) angle synchrotron X-ray scatterings[7] applied to samples

Received: May 10, 2011
Published: August 22, 2011

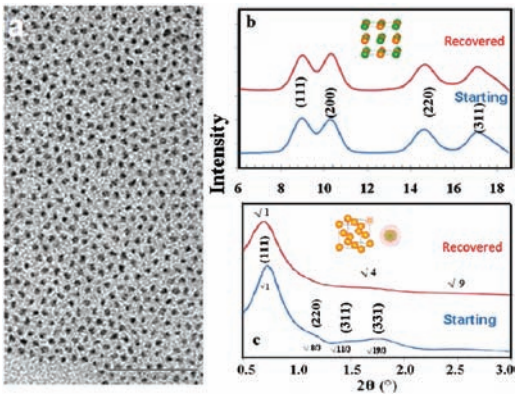

Figure 1. Synthesized PbS NPs and recovered samples: (a) Typical TEM image of starting NPs; (b) WAXS patterns showing a rocksalt-type cubic structure; and (c) SAXS patterns showing a face-centered-cubic arranged NP supercrystal with *Fm*3*m* and its transformation to a lamellar superstructure.

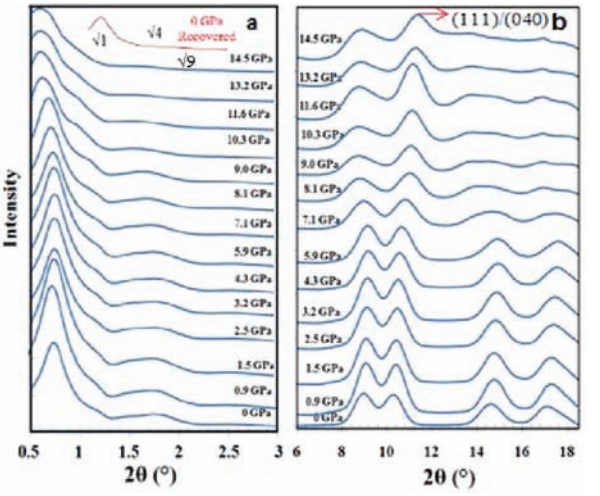

Figure 2. In situ pressure X-ray scattering patterns of NPs at λ = 0.533954 Å: (a) SAXS and (b) WAXS.

under pressure. Data were collected by both techniques on the same spot to directly monitor the kinetic development of (deviatoric) stress-tuned orientation and attachment of PbS NPs. High-resolution transmission electron microscopy (HRTEM) was supplemented to characterize the resultant structure and texture, offering a direct image of the developed crystallographic orientation and coalescence. We report on a deviatoric stress driven synthesis and in situ growth mechanism of large single-crystal PbS nanosheets with a lamellar mesostructure via a consequence of rotation, alignment and attachment, and coalescence of NPs.

PbS NPs passivated by oleic acid (OA) at surfaces were synthesized using a standard approach described by Nagel et al.[8] After purification, NPs were redispersed in anhydrous chloroform. A TEM image shows that NPs have an average grain size of 3.5 nm (Figure 1a). Synchrotron X-ray diffraction confirmed that NPs crystallize in a rocksalt (RS) structure (*Fm*3*m*) with a unit cell parameter of a_0 = 5.9502 Å (Figure 1b). NPs were drop-casted directly on the tip of one diamond anvil through a 200 μm diameter stainless steel gasket hole that serves as a sample chamber. After the sample was dried in air, several ruby chips were loaded on the top of the sample from the center to the edge in the hole for monitoring pressure and estimating deviatoric stress and pressure gradient, which can be determined independently using widths of ruby emissions and variation of wavelengths of ruby emissions, respectively. Without pressure medium, another perfectly prealigned diamond anvil was used to close the sample chamber for pressurization. This sample-loading approach in a diamond anvil cell (DAC) offers a nonhydrostatic environment, enabling a number of efficient inter-NP interactions and a rapid generation of pressure gradient and deviatoric stress. In situ SAXS and WAXS measurements on the same spot of samples were conducted at B_2 station of CHESS upon compression of the samples in a pressure cycle from 0 to 14.5 GPa and back to ambient.

Evaporation of anhydrous chloroform from the drop-casted NP-solution sample on the diamond anvil tip results in a rapid aggregation and periodic ordering of PbS NPs. At ambient conditions, a powder featured SAXS pattern (Figure 1c) shows that the aggregated NPs consist of randomly nucleated supercrystal (SC) domains. For all experiments, $q = (4\pi \sin \theta)/\lambda$ (in 1/Å), where θ and λ are the scattering angle and wavelength of the X-ray used, respectively. The observed peaks from SC powders at the positions (q) relative to the first strongest peak (q_0) at $d_{SC}(111)$ = 4.3 nm follow a noticeable correlation of q/q_0 = $\sqrt{1}/\sqrt{8}/3/\sqrt{11}/3/\sqrt{19}/3$, indicative of a face-centered-cubic arranged superlattic structure with a unit cell parameter of a_0 = 7.45 nm (Figure 1c). Lack of SC(200) peak favors assignment of cubic superstructure to space group *Fd*3*m* rather than *Fm*3*m*. While OA molecules (straight length = ~1.8 nm, but slightly coiled and shorter in SC) are considered to cover NP surfaces, the nearest inter-NP distance of nucleated SC is estimated to be 5.3−7.1 nm, which corresponds to the sum of one NP diameter plus single or double the length of straight OA molecule, respectively. For the SC with a space group of *Fd*3*m* or *Fm*3*m*, the observed cell parameter of a_0 = 7.45 nm enables estimation of the nearest inter-NP distance as 3.2 or 5.3 nm, respectively, suggesting that *Fm*3*m* is the correct space group for the nucleated SC (Figure 1c). The SC(200) peak may have been lost in the noise of an increased background at the overlapping range between the two nearby broad peaks of SC(111) and SC(220). Applying the full width at half-maximum (fwhm) of the SC(111) peak to the *Scherrer* equation, the SC particle size was estimated ~21 nm.

In situ pressure SAXS patterns indicate that, upon continuous increase of pressure, the observed peaks shift to higher angle, indicative of a pressure-induced shrinkage of inter-NP distance (Figure 2a). But when pressure is higher than 7.1 GPa, inter-NP distances start to increase (SI Figure 14). Slight enhancement of SC(220) intensity emerges as one significant sign for the occurrence of deviatoric stress across the sample. Upon enhancement of deviatoric stress, a SC(110)-preferred orientation was developed in parallel to the compression axis. When NPs approach closer within each SC(110) plane along the compression axis (e.g., SC[110]-normal), inter-NP-filled OA molecules travel radially, and accordingly expand the inter-NP spacing in one SC ⟨110⟩ direction that is perpendicular to the compression axis and has developed a large pressure gradient with enhanced deviatoric stress. At 11.6 GPa, several groups of nearby SAXS peaks start to merge; at 14.5 GPa, the number of peaks is reduced to 3. Three remaining peaks display a linear correlation of q/q_0= 1/2/3, indicating the formation of a lamellar mesostructure (see later section and Supporting Information (SI) for detail). Upon release of pressure to ambient condition, the lamellar mesostructure was well preserved (Figure 1c).

In situ pressure WAXS patterns (Figure 2b) offer two significant features: upon compression, RS(111) and RS(200) show slightly enhanced intensity but do not show significant widening of fwhm;

dx.doi.org/10.1021/ja204310b |*J. Am. Chem. Soc.* 2011, 133, 14484–14487

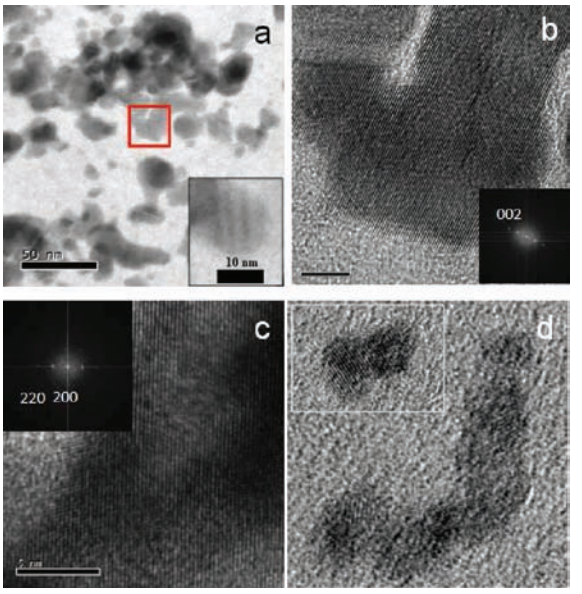

Figure 3. TEM images of the recovered sample from high pressure: (a) nanosheet and lamellar structures with a width of 2.5 nm (inset); (b) HRTEM image of the red-marked area in (a) showing (002) planes; (c) HRTEM image of nanosheets with ⟨100⟩ zone; and (d) two dominant attachments through (100) and (110) orientation and the fused NP dimer (inset).

RS(220) displays a noticeable widening of fwhm but does not show weakened intensity. These pressure-induced variations indicate a pressure-induced formation of RS(220) in-plane deviatoric stress. At 7.1 GPa, the NP begins to transform from RS to an orthorhombic (OR) phase. This pressure is significantly greater than the transition pressure of 2.2−2.5 GPa observed in bulk, and close to 8.1−9.2 GPa observed in 7 nm NPs with hydrostatic compression.[9] At 11.6 GPa, the high pressure OR phase displays a dramatic enhancement of the scattering intensity of OR(111) and OR(040), indicative of an increase of OR(111) and OR(040) planes. Previous studies on bulk PbS demonstrated that both OR(111) and OR(040) planes originate from a pressure-induced distortion of RS(200) and RS-(220).[9] It is thus suggested that the deviatoric stress driven attachment and coalescence of NPs undergo an intermediate process toward sharing a common crystallographic plane of either RS(220) or RS(200) or both. The atomic-scale phase transformation is completed at a pressure of 11.6−13.2 GPa. Following a transition-induced stress release (e.g., buffering effect between low and high pressure phase), deviatoric stress increased again. The increased deviatoric stress resulted in reduced intensity and increased widening of fwhm of the diffraction peaks of the OR phase. The high pressure OR phase remains stable to the peak pressure of 14.5 GPa. Releasing pressure to ambient conditions resulted in transformation back to the RS phase.

HRTEM characterizations further confirmed the formation of the enlarged 2D single-crystal structures and the crystallographic orientation and attachment. A typical TEM image in Figure 3a shows that 2D nanosheet dominates the morphologies. Nanosheets have a prevailing length scale of 15−30 nm, consistent with the initial SC particle size. Inset in Figure 3a shows a typical texture with nanosheets edge-on in which the periodically arranged nanosheets have a regular width of 2.5 nm, slightly smaller than the NP size of 3.5 nm. Figure 3b,c reveals that both RS(200) and RS(220) guide the orientation of attachment and growth of

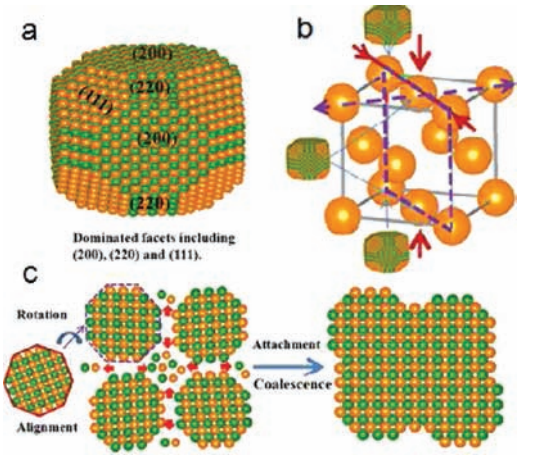

Figure 4. Schematic demonstration for the oriented attachment model: (a) reconstructed PbS NP terminated at surface by (200), (220), and (111) facets; (b) uniaxial compression and resulted compression and tension in a plane normal to the oriented SC(110); (c) left, stress-tuned rotation and alignment along SC(110) seen from downzone RS[100]; right, coalesced single crystal sheet via oriented attachments.

nanosheets. The dimers and trimers which formed at lower pressures at the edge of the sample chamber provide additional and straightforward evidence for the above-claimed conclusion (Figure 3d). These observations clearly show the kinetic process of oriented attachment: PbS NPs align their RS(220) and RS(200) planes with corresponding planes in neighboring NPs. As deviatoric stress is enhanced, NPs become attached through oriented RS(220) and RS(200) planes, and eventually coalesce into 2D single-crystal nanosheets. RS(200) fringes have a *d*-spacing of ∼2.8 Å (Figure 3b, c) and are smaller than the bulk value of 3.0 Å, suggesting that the nucleated nanosheets are highly strained.

In situ pressure SAXS and WAXS and HRTEM characterizations enable us to determine the growth route of 2D single-crystal PbS nanosheets from the short-range ordered NPs. Based on the theories of Wulff crystallographic reconstruction and surface energy minimization, the proposed morphology and surfaces of PbS NP are represented in Figure 4a. Three low surface energy facets of RS{200}, RS{220}, and RS{111} form at PbS NP surfaces, in agreement with previous HRTEM observations and morphological analyses.[8] At an early stage, compression of PbS NPs generates a small pressure gradient and deviatoric stress across the sample. Deviatoric stress acts as a driving force that develops a SC(110)-preferred orientation in the cubic SC with SC(110) planes parallel to the compression axis. Simultaneously, NPs in each SC(110) plane rotate, so their RS(200) and RS(220) planes become parallel to the corresponding planes in neighboring NPs. As a result, corresponding crystallographic planes join, leading to development of preferential orientation within each NP supercrystal particle (Figure 4b). Above 6.0 GPa, pressure gradient increases and deviatoric stress is enhanced, so the OA molecules passivated at RS(220) and RS(200) surfaces are squeezed out from the uniaxial compression and travel radially. Upon increasing pressure, enhanced deviatoric stress produces an anisotropic stress field that includes two compression directions and one tensile direction (SI Figure 13). In one direction within the plane normal to the compression axis, tensile stress acts to drive the movement of OA molecules which, in turn, results in a reverse expansion of inter-NP distance in one SC ⟨110⟩ direction (SI Figure 13,14). At 11.6 GPa, oriented NPs inside each SC particle completely coalesce together

into a group of single-crystal nanosheets that simultaneously stack into a periodically ordered lamellar mesostructure (Figure 4c). This is consistent with the observed constant inter-NP distance at pressures above 11.6 GPa (SI Figure 14) because no ligand is left within the completely coalesced SC(110) planes. Unlike the NP core, NP surfaces contain a larger ratio of atoms that have lower bonding numbers. Thermodynamically, surface atoms (e.g., Pb and S) have much greater chemical reactivity and structural instability than the atoms of NP core. Deviatoric stress resulting from increasing pressure drives these active surface atoms to move around, eliminating defects and stacking faults, filling voids, closing the vacant porous sites between interconnected NPs, and ultimately forming single-crystal nanosheets to reach a low energy structure (Figure 4c).

Features of crystal nucleation and crystal growth are often attributed to stress when in fact they may be due to strain involving mechanisms like those described above. In an effort to separate the effects of strain from those of stress as the more important driving mechanism in some phase transitions, Bassett et al.[10] conducted DAC experiments in which ungasketed silicate samples were squeezed to pressures in excess of the transition pressure and then heated gradually until visual changes revealed the presence of the high-pressure phase. In all the experiments on orthosilicates carried out this way, the high-pressure phase made its first appearance in the portion of the sample where strain was greatest (where the sample was actively flowing), not where the pressure was highest. It was only at higher temperatures that the portion of the sample at higher pressure but lower strain also underwent the phase transition. This suggests that both stress and strain play a role that results in the ultimate formation of the single-crystal nanosheets observed in this study.

The surface chemistry and crystallographic structure of PbS NPs provide a reasonable explanation for the deviatoric stress driven orientation and attachment via alignment of the two preferred crystallographic planes of RS(220) and RS(200). PbS NPs have a RS structure in which the surface-terminated facets display strong anisotropic polarization from one to another. For binary compounds with a RS structure, PbS behaves like PbSe, MgO, and NiO. Without coverage of organic molecules, unreconstructed {111} surfaces have a higher surface energy than {200} and {220} surfaces.[11,12] Upon coverage of organic molecules at surfaces, reconstructed {111} surfaces reduce energy more than an order of magnitude, and accordingly, reconstructed {111} surfaces become more stable than {200} and {220} surfaces.[11,12] The ligand-tuned dramatic change of surface energy has been observed in previous studies on MgO, NiO, and PbSe.[11,12] Recent theoretical modeling on PbS NPs indicates that passivation of $(CH_3COO)_2$ at {200} and {111} surfaces produces a similar variation of surface energy.[13] Correlating these results to the OA-passivated PbS NPs, reconstructed {111} surfaces of PbS NPs are expected to be more stable than {220} and {200} surfaces. Thermodynamically, PbS NPs favor a self-catalyzed energy-minimization process toward a stable low energy structure. One possible way in a static system is that the aggregated NPs precede a series of oriented attachments and fusions to eliminate high energy surfaces and interfaces and reduce surface energy. In this work, given a driving force considerably accelerates this dynamic process for quick alignment, orientation, and coalescence of high surface energy surfaces of RS{200} and RS{220} of nearby NPs to nucleate single-crystal nanosheets with reduced energy.

The growth mechanism and stress-driven synthesis offer an alternative tool for design and fabrication of advanced functional materials with controlled mesostructure, enhanced or newly manifested anisotropic properties. Several applications can be enabled: (1) control the ratio of surface ligands to embedded hard core materials for fabrication of matrix-mediated NP building blocks with single-crystal-like mesostructure, similar to the bioinspired or sol−gel assisted synthesis of single crystal, with enhanced mechanical properties;[4] (2) modify pressure medium and govern the magnitude of deviatoric stress to make large-scale nanorod, nanoring, and nanoplate that hold size-related quantum properties; (3) create highly strained nanoscale networks for development and application of strain nanotechnology.

■ ASSOCIATED CONTENT

Supporting Information. Experimental details and additional data. This material is available free of charge via the Internet at http://pubs.acs.org.

■ AUTHOR INFORMATION

Corresponding Author
zw42@cornell.edu

■ ACKNOWLEDGMENT

CHESS is supported by the NSF award DMR-0936384. H.F. thanks the DOE for funding.

■ REFERENCES

(1) (a) Schliehe, C.; Juarez, B. H.; Pelletier, M.; Jander, S.; Greshnykh, D.; Nagel, M.; Meyer, A.; Foerster, S.; Krnowski, A.; Klinke, C.; Weller, H. *Science* **2010**, *329*, 550. (b) Son, J. S.; et al. *Angew. Chem., Int. Ed.* **2009**, *48*, 6861. (c) Tang, Z.; Zhang, Z.; Wang, Y.; Glotzer, S. C.; Kotov, N. A. *Science* **2006**, *314*, 274. (d) Cho, K. S.; Talapin, D. V.; Gaschler, W.; Murray, C. B. *J. Am. Chem. Soc.* **2005**, *127*, 7140.

(2) (a) Wu, H.; Bai, F.; Sun, Z. C.; Haddad, R.; Boye, D.; Wang, Z. W.; Fan, H. *Angew. Chem., Int. Ed.* **2010**, *49*, 8431. (b) Wang, Z. W.; Wen, X. D.; Hoffmann, R.; Son, J. S.; Li, R. P.; Fang, C. C.; Smilgies, D. M.; Hyeon, T. *Proc. Natl. Acad. Sci. U.S.A.* **2010**, *107*, 17119.

(3) (a) Penn, R. L.; Banfield, J. F. *Science* **1998**, *281*, 969. (b) Zhou, Y.; Antonietti, M. *J. Am. Chem. Soc.* **2003**, *125*, 14961. (c) Yu, J. H.; Joo, J.; Park, H. M.; Baik, S.; Kim, Y. M.; Kim, S. C.; Hyeon, T. *J. Am. Chem. Soc.* **2005**, *127*, 5662.

(4) Colfen, H.; Antonietti, M. *Angew. Chem., Int. Ed.* **2005**, *44*, 5676.

(5) (a) Mann, S., *Biomineralization*; Oxford Univ. Press: Oxford, 2001. (b) Banfield, J. F.; Welch, S. A.; Zhang, H.; Ebert, T. T.; Penn, R. L. *Science* **2000**, *289*, 751. (c) Meldrum, F. C.; Colfen, H. *Chem. Rev.* **2008**, *108*, 4332.

(6) Wang, Z. W.; Guo, Q. X. *J. Phys. Chem. C* **2009**, *113*, 4286.

(7) Wang, Z. W.; Chen, O.; Cao, C. Y.; Finkelstein, K.; Smilgies, D. M.; Lu, X.; Bassett, W. A. *Rev. Sci. Instrum.* **2010**, *81*, 093902.

(8) Nagel, M.; Hickey, G. S.; Frömsdorf, A.; Kornowski, A.; Weller, H. Z. *Phys. Chem.* **2007**, *221*, 427.

(9) (a) Grzechnik, A.; Friese, K. *J. Phys.: Condens. Matter* **2010**, *22*, 095402. (b) Knorr, K.; Ehm, L.; Hytha, M.; Winker, B.; Depmeier, M. *Eur. Phys. J. B* **2003**, *31*, 297. (c) Podsiadlo, P.; Lee, B.; Prakapenka, V. B.; Krylova, G. V.; Schaller, R. D.; Demortiere, A.; Shevchenko, E. V. *Nano Lett.* **2011**, *11*, 579.

(10) (a) Wu, T.-C.; Bassett, W. A.; Burnley, P. C.; Weathers, M. S. *J. Geophys. Res.* **1993**, *98*, 19767–19776. (b) Burnley, P. C.; Bassett, W. A.; Wu, T.-C. *J. Geophys. Res.* **1995**, *100*, 17715–17723.

(11) Fang, C, M.; Van Huis, M. A.; Vanmaekelbergh, D.; Zandbergen, H. W. *ACS Nano* **2010**, *4*, 211.

(12) Wander, A.; Bush, I. J.; Harrison, N. M. *Phys. Rev. B* **2003**, *68*, 233405.

(13) Choi, J. J.; Bealing, C. R.; Bian, K. F.; Hughes, K. J.; Zhang, W. Y.; Smilgies, D. M.; Hennig, R. G.; Engstrom, J. R.; Hanrath, T. *J. Am. Chem. Soc.* **2011**, *133*, 3141.